LPDA Calibration Using an UAV for Synthesizing UWB Impulses

K. Muzalevskiy

***Abstract*—In this letter, the possibility of synthesizing ultra-wideband (UWB) impulses with a conventional log-periodic dipole antenna (LPDA) mounted on a quadrotor unmanned aerial vehicle (UAV) was demonstrated. The formation of impulses using LPDA (bandwidth from 427 MHz to 1.01 GHz) with a duration of 1.9 ns, containing one period of field oscillations, became possible due to compensation of amplitude and phase-frequency distortions introduced by the antenna into radiated and received impulses. Compensation for these distortions was carried out by inverse filtering method after calibrating the antenna-feeder path at various heights UAV hovering above the reference reflector (brass mesh). The conductive carbon elements of UAV, located in the near field of the antenna, are indirectly taken into account during the calibration of antenna-feeder path parameters and do not introduce significant distortions into the generated impulses. The suggested method of synthesizing UWB impulses can find application in environmental remote sensing and can also be used to sharpen fronts of impulses radiated\received with LPDA.**

***Index Terms*—Log-periodic dipole antenna (LPDA), complex antenna transfer function, complex antenna return loss, ultra-wideband (UWB) impulses, impulse radiation, unmanned aerial vehicle (UAV).**

I. Introduction

With ultra-wideband (UWB) shocking or continuous excitation of log-periodic dipole antennas (LPDA), radio impulses are emitted with a large number of high-frequency aperiodic oscillations, the frequency of which decreases with time [1]-[3]. This phenomenon occurs due to the construction features of LPDA in the form of two-wire transmission lines with symmetrical vibrators connected to it, resonating at different frequencies (with earlier excitation of high-frequency dipoles than low-frequency dipoles). As a result, the phase center of the antenna shifts, and a time delay between the high-frequency and low-frequency components of the impulse spectrum, radiated by LPDA happens [4]. This phenomenon does not allow LPDA radiates impulses, containing several oscillations of an electromagnetic field.

In this connection, new antenna construction was developed using the linear law of changing the resonant frequencies of adjacent dipoles and feeding the antenna from the large end (avoiding interference between the field excited by coaxial cable and the main radiated field). These construction changes make it possible to synthesize UWB impulses [2]. To minimize the amplitude- and phase-frequency distortions introduced by LPDA into the radiated impulses, additional time-delay chains (delay lines) [3], [5], and specific construction of sinusoidal dipoles and dielectric-loaded coverages are used [6]. In [7], the method for calibrating the phase-frequency characteristic of LPDA in a frequency range from 400 MHz to 1200 MHz [7] was proposed to compensate for the frequency dispersion of position of LPDA phase center. These approaches significantly reduce the dispersion distortions introduced by LPDA into radiated impulses. In [8], under laboratory radar stand, the possibility of UWB impulses synthesizing was demonstrated using conventional LPDA [9]. The approach in [8] is close to the ideas described in [10], [11]. However, in [10], a nondispersive antenna was used, and the amplitude and phase-frequency characteristics of the antenna were not corrected. In [11], a broadband dipole antenna and the hardware correction of its frequency response unevenness were used to synthesize a nanosecond video impulse by means of the train of 4 radio impulses.

In this letter, the possibility of synthesizing UWB impulses by LPDA placed on an UAV is investigated. In contrast to [8], where the studies were carried out in the near and intermediate field regions of LPDA, the flight altitude of UAV makes it possible to synthesize UWB pulses in the far field. In the approach [8], the antenna-feeder path was represented as a model of a two-port linear network with S-parameters. This model contained a frequency-independent parameter (phase center of the antenna) and two frequency-dependent functions: complex antenna return loss in an "empty room" (CARL) and two-way complex antenna transfer functions (CATF), which need calibration. In the first stage, the technique [8] required finding CARL and CATF when placing the antenna only at several heights above the metal sheet. On the second stage, the phase center of antenna was found in the course of solving the minimization problem. In the approach proposed here, due to the high flight altitude of UAV, there is no need to accurately determine the position of the antenna phase center, as required by the methods [8], [12]. As a result, the antenna-feeder path model can be linearized, and the problem of finding CARL and CATF can be solved using a rigorous mathematical approach in the form of the least-squares problem. The placement of LPDA on UAV significantly changes the antenna radiation conditions,

Manuscript received March 18, 2023. The investigation supported by the Russian Science Foundation and the Krasnoyarsk Regional Science Foundation, project № 22-17-20042. K. V. Muzalevskiy is with the Kirensky Institute of Physics Federal Research Center KSC SB RAS, 660036 Krasnoyarsk, Russia (e-mail: rsdkm@ksc.krasn.ru).

compared to the experiments on the radar stand [8]. The possibility of synthesizing UWB impulses containing one period of field oscillation is not obvious due to the placement of conductive UAV carbon structures in the antenna near field region (including rotating propellers that create random configurations of reflectors), which requires additional research.

II. Calibration of LPDA and Synthesizing UWB Impulses

A. Model of Antenna-Feeder Path

Let printed LPDA be attached to UAV in such a way that its main lobe is oriented at a normal angle to a reflective flat surface (see Fig. 1). Realizing the continuous-wave monostatic radar system, the antenna port was connected to a vector network analyzer (VNA). The antenna-feeder path will be represented as a four-terminal network [8], [12]-[14] characterized by scattering S-matrix:

$$r(f,d) = r_0(f) + \frac{G(f,d)Tr(f)}{1-S_{22}(f)G(f,d)}, \quad (1)$$

where $r(f,d)$ is CARL measured by VNA, when LPDA is placed over a flat reflected surface, $r_0(f)$ is CARL in «empty room», f is the wave frequency, $Tr(f)$ is CATF, $S_{22}(f)$ is CARL from the antenna towards the main lobe direction, $G(f,d)$ is Green's function for a half-space (a point source placed in the LPDA phase center), d is the distance between a reflection plane and the phase center of LPDA. In (1) the exact position of the phase center d (see Fig. 1) and empirical functions of $r_0(f)$, $Tr(f)$, $S_{22}(f)$ needs to be defined.

B. Method of LPDA Calibration

Considering that the flight altitude of an UAV can always be set significantly greater than the maximum wavelength radiated wave by the antenna, then, unlike [12] in (1), the exact analytical expression for Green's functions can be derived in the far-field approximation [15]:

$$G(f,d) = R(f)g(f,d),\ g(f,d) = e^{4\pi i\frac{f}{c}d}/(8\pi d), \quad (2)$$

where $R(f)$ is the Fresnel's reflection coefficient from a flat surface (normal incidence). For the same reason, it is possible to neglect the waves reflected from LPDA towards to flat surface and re-reflected back to the antenna ($S_{22}(f)\approx 0$). In contrast to [8] and [12] in the proposed approach, the phase center of the antenna does not need to be precisely determined. Calculations show (see Fig. 2) that the shift of the antenna phase center by $\Delta\pm 0.1$ m from the true value leads to a relative error of less than ~10% in the calculation of the Green's function (2), when the UAV flight height is above 1 m. Further, it will be assumed that the position of the antenna phase center, d, is known and given with an absolute error of no more than ± 0.1 m. As a result, based on the assumptions made, the equation (1) can be linearized and written as:

$$r(f,d) = r_0(f) + R(f)g(f,d)Tr(f). \quad (3)$$

$r_0(f)$, $Tr(f)$ will be found from $r(f,d)$ measurements at the antenna placed at different heights above the calibration reflector (metal screen), assuming $R(f) \equiv -1$ in model (3).

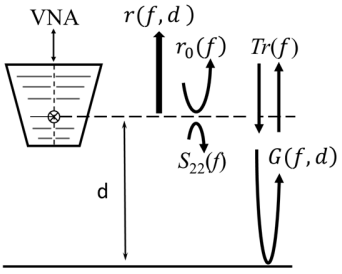

Fig. 1. Diagram of LPDA model decomposition. Phase center of LPDA is depicted by circle with cross.

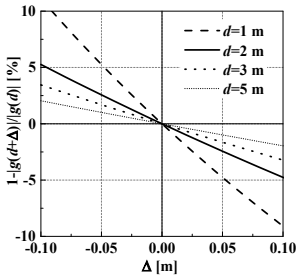

Fig. 2. The error in the calculation of Green's function at different altitudes and shifts of antenna phase center Δ.

The method of antenna calibrating, when it is placed at different heights above the metal reflector, was widely used earlier [8], [12]-[14], [16], [17]. Having N measured values of $r(f,d_n)$ at heights of d_n, n=1, …, N, the overdetermined system of N linear equations can be obtained:

$$B = Ax,$$
$$B = \begin{pmatrix} r(f,d_1) \\ \vdots \\ r(f,d_N) \end{pmatrix}, A = \begin{pmatrix} 1 & -g(f,d_1) \\ \vdots & \vdots \\ 1 & -g(f,d_N) \end{pmatrix}, x = \begin{pmatrix} r_0(f) \\ Tr(f) \end{pmatrix}. \quad (4)$$

The overdetermined system of linear equations (4) can be solved for each frequency f in the sense of a least-squares problem [18]: $\min_{x(f)} \|Ax(f) - B\|_2$, $x(f)=(A^TA)^{-1}A^TB$, where A^T is the transpose of matrix A. Based on the found $r_0(f)$, $Tr(f)$ and model (3), inverse filtering can be performed to minimize the amplitude and phase-frequency distortions introduced by LPDA into the synthesized UWB impulses.

C. Synthesizing UWB Impulses

Based on the model (3), the analytical signal $\dot{s}(t,d_n)$ of the synthesized UWB impulses can be calculated using the Fourier transform:

$$\dot{s}(t,d_n) = -\int_{f_{min}}^{f_{max}} df\, W(f)\{r(f,d_n) - r_0(f)\}e^{-2\pi ift}, \quad (5)$$

where t is the time, f_{min} and f_{max} are the minimum and maximum frequency in the spectrum of synthesized UWB impulses, $W(f)=K_\sigma(f)/Tr(f)$ is the correcting function, $K_\sigma(f)=\exp(-0.5[(f-0.7)/\sigma]^2)$ is the Gauss window function (bandwidth of order 1 GHz at -6 dB level), $\sigma = \left(2\sqrt{2ln2}\right)^{-1}$. The Gauss window function was used to reduce the "noise" pulsations level relative to the main lobe of the synthetized impulses. Integral (5) was calculated by means of the Gauss interpolation quadrature formula (with 24th nodes and 40th segments subdivisions of integrand) [19]. Finally, the time shape $s(t,d_n)$ and the upper envelope $s^a(t,d_n)$ of the synthesized UWB impulses were calculated based on the formulas:

$$s(t,d_n) = 2Re\,\dot{s}(t,d_n),\ s^a(t,d_n) = 2|\dot{s}(t,d_n)|. \quad (6)$$

III. Results and Discussion

A. Description of Experimental UAV Platform

UWB monostatic radar (see Fig. 3) was assembled with portable Planar CABAN R60 VNA and printed LPDA [8], [9]. The UAV radar is housed on a quadrotor (Tarot 650 frame) equipped with a LIDAR-Lite v3 laser rangefinder (distance measurement error ±1 cm). Relative to the phase center of LPDA [8], the calibration plane (zero distance) of the laser rangefinder appeared to be equal to 4.4 cm higher. UAV was managed by Pixhawk 4 flight controller and LattePanda V1 microcomputer. The developed software (based on python, MAVLink MAVSDK) allows to synchronize of the UAV flight and CABAN R60 reflectometric measurements. The CABAN R60 VNA was controlled programmatically (Python) using SCPI (Standard Commands for Programmable Instruments) text commands via TCP/IP protocol (STREAM socket). The jMAVSim simulator was used to verify all algorithms for the operation of the equipment and flight tasks.

Fig. 3. UAV over a brass mesh during antenna calibration. 1) LPDA, 2) LIDAR-Lite v3, 3) VNA CABAN R60.

B. CARL and CATF of LPDA Measured with UAV

In line with the proposed technique, $r(f, d_n)$ was measured at different UAV hovering heights above the brass mesh reflector (d_1=0.87m, d_2=1.16 m, d_3=1.47 m, d_4=2.27m, d_5=2.59 m, d_6=3.04 m, d_7=4.57 m, and d_8=5.71 m). The total size of the reference reflector was 6m x 7m (see Fig. 3). To study the influence of UAV propellers rotation (random factor) on the retrieval values of CARL and CATF, $r(f, d_n)$ was measured five times (run 1,…, run 5) with a delay of 1 second at each altitude. For each runs CARL, $r_0(f)$, and CATF, $Tr(f)$, were retrieved based on equation (4). As an example, Fig. 4 shows the CARL and CATF measured using UAV for three runs (see blue lines) and the corresponding values measured on the radar stand [8] (red lines). Magnitude $|r_0(f)|$ and phase $\angle r_0(f)$ measured with UAV are almost the same for different runs (see Fig. 4a, blue lines). The Magnitude $|Tr(f)|$ and phase $\angle Tr(f)$ measured with the UAV for different runs vary in the range of ±1.9 dB and ±0.7 rad, respectively (see Fig. 4b, blue lines), in terms of standard deviation. The only reason for these variations may be random reflections between rotating propellers and LPDA in the individual runs. In the frequency range from 427 MHz to 1.01 GHz, CARL and CATF measured on the radar stand [8] (see Fig. 4, red line) is approximately 5-7 dB lower compared to the CARL and CATF measured using the UAV (see Fig. 4, blue lines).

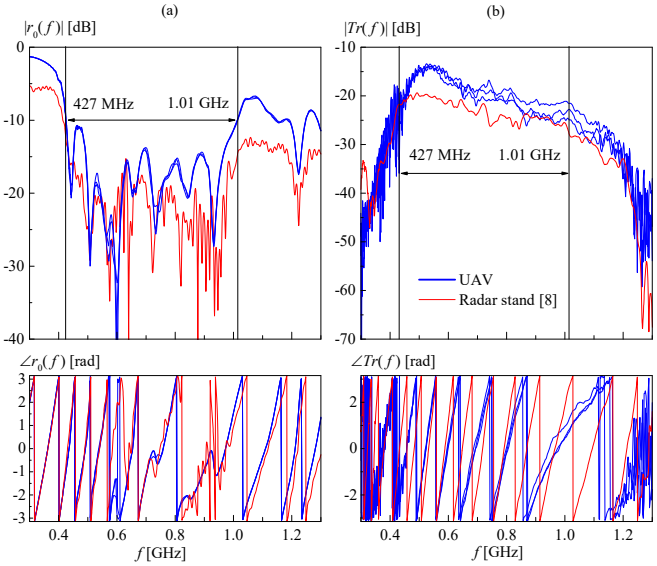

Fig. 4. Magnitude $|\cdot|$ and phases $\angle\cdot$, CARL, $r_0(f)$, and CATF, $Tr(f)$, measured on radar stand [8] (red lines) and with the UAV (blue lines, only three lines are shown to eliminate the strong blurring of the lines). In Fig. 4a and 4b, the arrows mark the LPDA bandwidth from 427 MHz to 1.01 GHz at a level of -10 dB.

This is due to additional wave attenuation in the 8m cable (TEW-L208) that was used to connect the antenna to the VNA in the experiments on the radar stand compared to the 0.5m cable (RG178) on the UAV. The CARL phases measured on the radar stand (see Fig. 4a, red line) and using the UAV (see Fig. 4a, blues) have close frequency dependences, and the corresponding CATF phases differ significantly (see Fig. 4b, red and blue lines). Apparently, this is due to the conductive carbon elements of the UAV located in the near field of the antenna. As a result, the antenna matching with free space is worsened, which leads to observable phase shifts, especially for CATF. A comparison of the measurement results (see Fig. 4) shows that CARL and CATF of the LPDA, measured on a radar stand, cannot be used to quantify CARL and CATF of the placed on a UAV LPDA.

C. Synthesizing UWB Impulses from UAV

Using CARL and CATF averaged over five runs, UWB impulses were synthesized using formula (5) with f_{min}=0.2 GHz and f_{max}=1.3 GHz. As an example, Fig. 5 shows the time shapes of impulses calculated with and without ($W(f)$=1) correction function for UAV hovering heights of d_2=1.16m and d_8=5.71m above the brass mesh. The duration (full width at half-maximum of an envelope) of synthesized UWB impulses appeared to be equal to 1.9 ns (see Fig. 5). The synthesized UWB pulses are more than five times shorter compared to the radio impulse synthesized without correction (see Fig. 5). The noise level outside the main lobe of synthesized UWB impulses is about -25÷-30dB (t>20ns, see Fig. 6). As an example, in Fig.

6 (dash lines) impulses, calculated using CARL and CATF measured for individual runs (see Fig. 4 blue lines) are given for UAV flight altitudes of d_2=1.16m and d_7=4.57m.

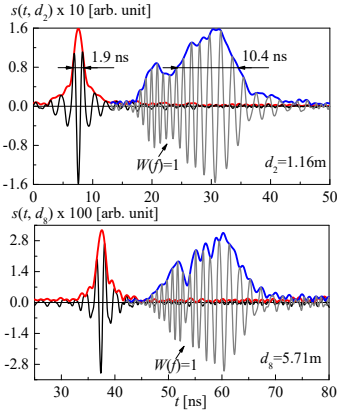

Fig. 5. Time shape of synthesized impulses.

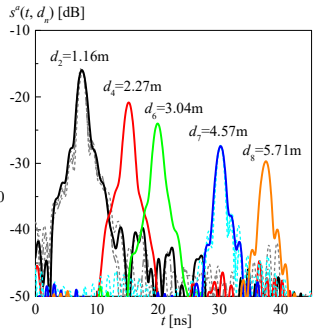

Fig. 6. Envelopes of synthesized impulses with using LPDA, measured at different hovering heights d_2-d_8 of UAV over brass mesh.

Fig. 6 shows that the variations of $r_0(f)$ and Tr(f) (see Fig. 4, blue lines) from run-to-run do not significantly impact the distortion of synthesized UWB impulses. Arrival times, t_{max}, of impulses (see Fig. 6, maximum of envelopes at 7.58ns, 15.21ns, 19.91ns, 30.19ns, and 37.57ns) linearly depend on the UAV hovering height, measured by the laser rangefinder: d=(-0.007±0.025)+(0.151±0.001) t_{max}. Therewith the root-mean-square error (RMSE) and coefficient of determination (R^2) are equal to 2.6cm and 0.999, respectively. The error of UAV altitude estimation through the impulse's arrival times is within the range measurement error of LIDAR-Lite v3 (1 cm) and the brass mesh surface roughness. Before the experiment brass mesh was smoothed out. However, individual surface irregularities could reach up to 1.5 cm relative to the level of the asphalt (which also had small vertical irregularities). Good linear accordance between t_{max} and d indicates that in the main lobe of synthesized impulses, there are no significant unaccounted wave re-reflections between the antenna and structural elements of the UAV due to incorrect calibration of the model (3). This also indicates the possibility of inaccurate assignment of the antenna phase center when finding the parameters of the model (3) and synthesizing impulses. The proposed method significantly improves the shape and duration of synthesized impulses in relation to [9].

V. Conclusion

This letter shows the possibility of amplitude- and phase-frequency characteristics correction for conventional LPDA (bandwidth from 427 MHz to 1.01 GHz) without making changes to its construction, which allows for radiated/received UWB impulses with a duration of 1.9 ns (containing several oscillations of an electromagnetic field) from a quadrotor UAV platform. This approach does not consider the radiation patterns of the antenna and can be applied only for one selected direction (the shape of impulses and the transfer function of the antenna have not been studied at different azimuthal and meridional angles, as well as depending on the polarization of radiation). It was shown that conductive carbon UAV's elements as well as the assignment error of the LPDA phase center (within 4.4 cm) do not significantly impact the possibility of synthesizing UWB impulses using LPDA on a quadrotor UAV. The suggested method was specifically designed for the applications of UWB impulses that are received/radiated by dispersive LPDAs in remote sensing from UAV quadrotor platforms.

References

[1] R. Burr, *et al.*, "Design and Implementation of a FMCW GPR for UAV-based Mine Detection," *IEEE MTT-S International Conference on Microwaves for Intelligent Mobility*, Munich, 2018, pp. 1-4.

[2] F. Merli, *et al.*, "Analysis, Design and Realization of a Novel Directive Ultrawideband Antenna," *IEEE Transactions on Antennas and Propagation*, vol. 57, no. 11, pp. 3458-3466, 2009.

[3] A. Khaleghi, *et al.*, "Impulse Radiating Log-Periodic Dipole Array Antenna Using Time-Reversal Technique," *IEEE Antennas and Wireless Propagation Letters*, vol. 10, pp. 967-970, 2011.

[4] W. Sörgel and W. Wiesbeck, "Influence of the Antennas on the Ultra-Wideband Transmission," *EURASIP Journal on Applied Signal Processing*, vol. 3, pp. 296–305, 2005. doi: 10.1155/ASP.2005.296.

[5] P. Rulikowski, J. Barrett, "Adaptive Arbitrary Pulse Shaper," *IEEE Microwave and Wireless Components Letters*, vol. 18, no. 5, pp. 356-358, 2008, 10.1109/LMWC.2008.922131.

[6] L. Chang, S. He, J. Q. Zhang and D. Li, "A Compact Dielectric-Loaded Log-Periodic Dipole Array (LPDA) Antenna," *IEEE Antennas and Wireless Propagation Letters*, vol. 16, pp. 2759-2762, 2017.

[7] García-Fernández M., et al. "Portable and Easily-Deployable Air-Launched GPR Scanner," *Remote Sensing*, vol.12, no. 11, Art. no. 1833, 2020. doi: 10.3390/rs12111833.

[8] K. Muzalevskiy, M. Mikhaylov and Z. Ruzicka, "Synthesizing of Ultra-Wide Band Impulse by means of a Log-Periodic Dipole Antenna. Case Study for a Radar Stand Experiment," *IEEE International Multi-Conference on Engineering, Computer and Information Sciences (SIBIRCON)*, Yekaterinburg, Russian Federation, pp. 1140-1143, 2022.

[9] M. A. Yarlequé, *et al.*, "FMCW GPR radar mounted in a mini-UAV for archaeological applications: First analytical and measurement results," *International Conference on Electromagnetics in Advanced Applications*, Verona, pp. 1646-1648, 2017.

[10] L. A. Robinson, W. B. Weir and L. Young, "Location and recognition of discontinuities in dielectric media using synthetic RF pulses," *Proceedings of the IEEE*, vol. 62, no. 1, pp. 36-44, 1974.

[11] M.I. Finkelstein, V.A. Kutev, "Probing of Sea Ice with a Sequence of Video Pulses," *Radio Engineering and Electronic Physics*, vo1.17, no.10, pp. 1680-1682, 1972.

[12] S. Lambot, *et al.*, "Modeling of ground-penetrating Radar for accurate characterization of subsurface electric properties," *IEEE Transactions on Geoscience and Remote Sensing*, vol. 42, no. 11, pp. 2555-2568, 2004.

[13] M. Nakhkash, *et al.*, "An improved calibration technique for free-space measurement of complex permittivity," *IEEE Transactions on Geoscience and Remote Sensing*, vol. 39, no. 2, pp. 453-455, 2001.

[14] V. A. Mikhnev, P. Vainikainen, "Single-reference near-field calibration procedure for step-frequency ground penetrating radar," *IEEE Transactions on Geoscience and Remote Sensing*, vol. 41, no. 1, pp. 75-80, 2003, 10.1109/TGRS.2002.808060.

[15] C. Y. Kee, C. Wang, "Far field approximation of half-space Green's function," *IEEE International Symposium on Antennas and Propagation & USNC/URSI National Radio Science Meeting*, San Diego, CA, pp. 1357-1358, 2017. doi: 10.1109/APUSNCURSINRSM.2017.8072721.

[16] G. G. Gentili and U. Spagnolini, "Electromagnetic inversion in monostatic ground penetrating radar: TEM horn calibration and application," *IEEE Transactions on Geoscience and Remote Sensing*, vol. 38, no. 4, pp. 1936-1946, 2000, doi: 10.1109/36.851775.

[17] S. A. Arcone, R. W. Larson, "Single-horn reflectometry for in situ dielectric measurements at microwave frequencies," IEEE Transactions on Geoscience and Remote Sensing, vol. 26, no. 1, pp. 89-92, 1988.

[18] G.H. Golub, C.F. van Loan, "*Matrix computations*." Third Edition. The Johns Hopkins University Press, Baltimore, MD, 1996, p. 694.

[19] M. Abramowitz, I.A. Stegun, "*Handbook of Mathematical Functions: with Formulas, Graphs, and Mathematical Tables*," National Bureau of standards, Applied mathematics series, no. 55, 1964, p.1082.